ISSN 1674-1056
http://cpb.iphy.ac.cn
http://iopscience.iop.org/cpb
中国物理 B
Chinese Physics
中国物理
Chinese Physics B

Ultrasonic beam focusing characteristics of shear-vertical waves for contact-type linear phased array in solid

Yu-Xiang Dai(戴宇翔), Shou-Guo Yan(阎守国), Bi-Xing Zhang(张碧星)

Citation: Chin. Phys. B . 2020, 29(3): 034304 . **doi:** 10.1088/1674-1056/ab69ed
Journal homepage: http://cpb.iphy.ac.cn; http://iopscience.iop.org/cpb

What follows is a list of articles you may be interested in

Micro-crack detection of nonlinear Lamb wave propagation in three-dimensional plates with mixed-frequency excitation

Wei-Guang Zhu(祝伟光), Yi-Feng Li(李义丰), Li-Qiang Guan(关立强), Xi-Li Wan(万夕里), Hui-Yang Yu(余辉洋), Xiao-Zhou Liu(刘晓宙)

Chin. Phys. B . 2020, 29(1): 014302 . **doi:** 10.1088/1674-1056/ab5931

Simulation of acoustic fields emitted by ultrasonic phased array in austenitic steel weld

Zhong-Cun Guo(郭忠存), Shou-Guo Yan(阎守国), Bi-Xing Zhang(张碧星)

Chin. Phys. B . 2019, 28(11): 114302 . **doi:** 10.1088/1674-1056/ab4d41

Lamb waves topological imaging combining with Green's function retrieval theory to detect near filed defects in isotropic plates

Hui Zhang(张辉), Hai-Yan Zhang(张海燕), Meng-Yun Xu(徐梦云), Guo-Peng Fan(范国鹏), Wen-Fa Zhu(朱文发), Xiao-Dong Chai(柴晓冬)

Chin. Phys. B . 2019, 28(7): 074301 . **doi:** 10.1088/1674-1056/28/7/074301

Influence exerted by bone-containing target body on thermoacoustic imaging with current injection

Yan-Hong Li(李艳红), Guo-Qiang Liu(刘国强), Jia-Xiang Song(宋佳祥), Hui Xia(夏慧)

Chin. Phys. B . 2019, 28(4): 044302 . **doi:** 10.1088/1674-1056/28/4/044302

Superwide-angle acoustic propagations above the critical angles of the Snell law in liquid–solid superlattice

Zhang Sai, Zhang Yu, Gao Xiao-Wei

Chin. Phys. B . 2014, 23(12): 124301 . **doi:** 10.1088/1674-1056/23/12/124301

Ultrasonic beam focusing characteristics of shear-vertical waves for contact-type linear phased array in solid*

Yu-Xiang Dai(戴宇翔)[1,2], Shou-Guo Yan(阎守国)[1,†], and Bi-Xing Zhang(张碧星)[1,2]

[1] *Key Laboratory of Acoustics, Institute of Acoustics, Chinese Academy of Sciences, Beijing* 100190, *China*
[2] *University of Chinese Academy of Sciences, Beijing* 100190, *China*

(Received 14 December 2019; revised manuscript received 9 January 2020; accepted manuscript online 10 January 2020)

We investigate the beam focusing technology of shear-vertical (SV) waves for a contact-type linear phased array to overcome the shortcomings of conventional wedge transducer arrays. The numerical simulation reveals the transient excitation and propagation characteristics of SV waves. It is found that the element size plays an important role in determining the transient radiation directivity of SV waves. The transient beam focusing characteristics of SV waves for various array parameters are deeply studied. It is particularly interesting to see that smaller element width will provide the focused beam of SV waves with higher quality, while larger element width may result in erratic fluctuation of focusing energy around the focal point. There exists a specific range of inter-element spacing for optimum focusing performance. Moreover, good beam focusing performance of SV waves can be achieved only at high steering angles.

Keywords: beam focusing, shear-vertical (SV) waves, contact-type linear phased array, solid

PACS: 43.20.+g, 43.35.+d, 43.38.+n **DOI:** 10.1088/1674-1056/ab69ed

1. Introduction

Over the last decades, the ultrasonic phased array technology has achieved considerable development, which now plays an important role in the fields of medical diagnosis,[1–4] nondestructive evaluation (NDE),[5–8] and so on. An ultrasonic phased array can be assembled by numerous piezoelectric elements that can be excited independently to generate ultrasonic waves. Thus, the principal advantage of phased arrays over traditional single-probe transducers is their flexible capability of beam controlling. Typically, the dynamical beam steering and focusing technology is the significant application of a phased array, which can be achieved by controlling the time delay and amplitude of excitation pulse on each element with a electronic hardware system. Due to the mature manufacturing technology and good beam controlling performance, linear phased arrays have the most extensive applications in NDE.

Generally, a contact-type transducer array is considered to primarily generate compressional waves (p-waves) in an inspection medium.[9] Therefore, the beam steering and focusing technology of p-waves for a linear phased array were deeply studied by many investigators with an assumption of fluid mediums.[10–15] However, a linear phased array using p-waves suffers a limitation from the steering angle, due to its poor performance at a higher steering angle.[8] This makes it hard to be employed to inspect the medium with complicated structures, such as the turbine disc head shown in Fig. 1(a), where the defects appear outside the available inspection area of p-waves.[16,17] This disadvantage motivates to propose the wedge transducer using shear-vertical (SV) waves, as shown in Fig. 1(b), whose fundamental principle is the wave mode conversion. The SV waves transmitting into the medium are generated by the refraction of p-waves excited by a transducer, which gives an access to perform inspections at a higher steering angle with the wedge transducer. Therefore, the wedge transducer array is typically applied in the detection of the component with a complicated structure. For instance, Crowther[16] summarized the applications of a wedge transducer array in NDE of power station. Ye *et al.*[18] carried out the research for employing linear phased arrays coupled with the wedge to detect flaws in the dissimilar metal welds. Lhémery *et al.*[19] introduced the modeling methods of the ultrasonic inspection for welds by using a wedge transducer array.

Despite the benefit of good performance at higher steering angles for a wedge transducer array, it also suffers some deficiencies. Firstly, a complicated field within the wedge will be generated by the multiple reflections of waves excited by the transducer array, which contaminates the received signals for imaging.[20] In previous works, some assumptions on the wedges were adopted to simplify the model, where the interference of reflected waves to received signals was neglected.[19,21] In practical circumstances, although the absorbing layer made of a lossy material shown in Fig. 2 is typically attached to the wedge in order to suppress the reflection, the reflected waves in the wedge can still make a non-negligible effect due to the limited absorption capability of most lossy materials. Secondly, the delay law of elements for beam focusing with the wedge transducer array is compli-

*Project supported by the National Natural Science Foundation of China (Grant Nos. 11774377 and 11574343).
†Corresponding author. E-mail: yanshouguo@mail.ioa.ac.cn
© 2020 Chinese Physical Society and IOP Publishing Ltd

cated. As shown in Fig. 2, the wave propagation path of each element for beam focusing is typically determined by using ray-tracing methods or Fermat's principle,[22] which makes it complicated to determine the time delay of each element. Thirdly, the wave mode conversion inevitably causes energy loss due to the acoustic impedance difference between the wedge and the inspection medium, which may result in the degradation of signal-to-noise ratio. Finally, the existence of wedge enlarges the overall size of the transducer array, which limits its application in the space-constrained components. In practical inspection, it is always desirable to minimize the overall size of the transducer array in an attempt to perform inspections for various components with complex structures, especially for the component without enough space available for the transducer array. In short, the wedge transducer array suffers some limitations in practical applications from the wedge.

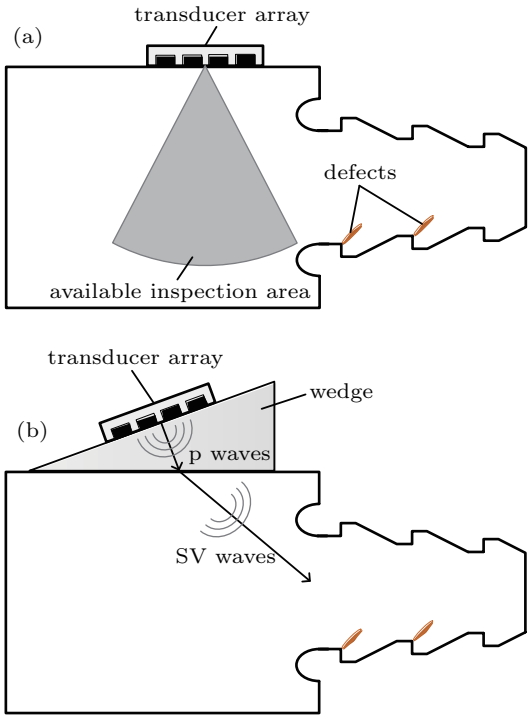


Fig. 1. A profile of the turbine disc head inspected (a) by a linear phased array using p-waves and (b) by a wedge transducer array using SV waves.

In most previous works, the SV waves directly generated by transducer array are always neglected, due to the traditional opinion that the conventional transducer array primarily generates p-waves.[9] In addition, the assumption of the fluid medium in the classical modelling approach of the field excited by the arrays also makes the SV waves neglected.[10–15] However, a number of recent studies illustrate the unique excitation and propagation mechanism of SV waves, which makes it possible to achieve beam focusing of SV waves with a contact-type transducer array.[20,23–25] For instance, Drinkwater *et al.*[20] pointed out that the SV waves with higher amplitude over p-waves could be generated by a contact-type transducer array in some special cases. Noroy *et al.*[24] improved the ultrasonic field generated by a laser array with the shear wave focusing technology. More recently, Zhang *et al.*[25] proposed the concept of ultrasonic focusing technology with multiple waves, whereas more in-depth analyses have not been given. Obviously, it is profoundly meaningful to study the beam focusing behavior of SV waves for a contact-type linear phased array. It is desirable for contact-type transducer arrays to achieve good beam focusing performance of SV waves at high steering angles and to overcome the shortcomings caused by the wedge. Additionally, another momentous aspect not taken seriously from most previous works is the transient performance of the linear phased array, where the transducer array was generally assumed to emit continuous waves.[15] In practical inspection, however, the elements are excited by the short-time pulse to generate transient waves, which make the field more complicated. In this paper, the elements are excited by the pulse with finite duration in an attempt to make the beam focusing field more realistic.

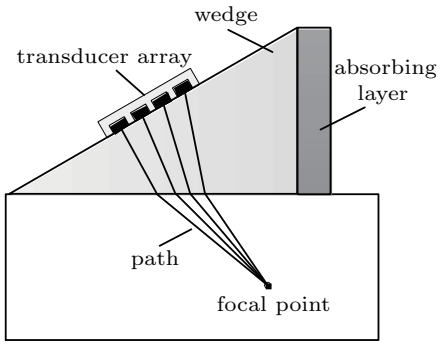


Fig. 2. A schematic diagram showing the typical beam focusing process of wedge transducer array.

The focus of this paper is on studying the transient beam focusing characteristics of SV waves for a contact-type linear phased array. The remainder of this paper is organized as follows. Section 2 gives the theoretical formulas for beam focusing field of SV waves excited by contact-type linear phased arrays. Section 3 shows the transient excitation characteristics of SV waves by numerical simulation. Also, the beam focusing performance of SV waves for various array design parameters is analyzed in detail. Finally, Section 4 summarizes the study.

2. Theoretical analysis

In this section, the theoretical formulas of the transient beam focusing field of SV waves excited by a linear phased array are given. In order to analyze the beam focusing characteristics of SV waves in detail, the radiation directivity function of beam focusing field is defined, which is an important aspect evaluating the focusing performance.

2.1. Field excited by a single element

Typically, the linear array behaves as infinitely long strip sources.[20] Hence, as shown in Fig. 3, the inspection medium can be assumed as a two-dimensional elastic half-space solid with a free boundary, where the element with width of $2a$ is placed on the surface. The Cartesian coordinate system (x, z) is introduced, where the origin is located at the center of the element. For convenience, the polar coordinate system (r, θ) is also introduced to analyze the beam directivity function later.

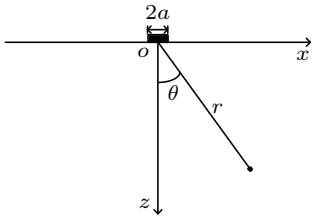


Fig. 3. Configuration of a single element source.

For the model given above, the wave equations can be written as

$$\begin{aligned}&\frac{\partial^2\varphi}{\partial x^2}+\frac{\partial^2\varphi}{\partial z^2}+c_{\mathrm{p}}^2\varphi=0,\\&\frac{\partial^2\psi}{\partial x^2}+\frac{\partial^2\psi}{\partial z^2}+c_{\mathrm{s}}^2\psi=0,\end{aligned}\tag{1}$$

where c_{p} and c_{s} are the velocities of p and SV waves, ϕ and ψ are the displacement potentials of p and SV waves.

The single element can be regarded as the normal surface-loading uniformly distributed on the free surface, hence the boundary conditions at $z=0$ can be written as

$$\begin{aligned}&\tau_{zz}(x,z=0,t)=\begin{cases}-f(t), & |x|\leqslant a,\\ 0, & |x|>a,\end{cases}\\&\tau_{zx}(x,z=0,t)=0,\end{aligned}\tag{2}$$

where τ_{zz} and τ_{zz} are the stresses, and $f(t)$ is the excitation source function loading on the element. The negative sign denotes that the force is loaded opposite to the external normal of the boundary.

This is a classical problem of wave motion in elastodynamics and can be solved by several methods. In this paper, with the angular spectrum method[26] based on 2-D Fourier transform, the solutions of displacement potentials can be obtained as follows:

$$\begin{aligned}\varphi(x,z,t)=&\frac{1}{2\pi}\int_{-\infty}^{\infty}F(\omega)\int_{-\infty}^{+\infty}\frac{2\sin(ka)}{\mu k}\cdot\frac{k_{\mathrm{s}}^2-2k^2}{G(k)}\\&\times\exp[\mathrm{i}(kx+\alpha z-\omega t)]\,\mathrm{d}k\mathrm{d}\omega,\\\psi(x,z,t)=&\frac{1}{2\pi}\int_{-\infty}^{\infty}F(\omega)\int_{-\infty}^{+\infty}\frac{2\sin(ka)}{\mu k}\cdot\frac{2k\alpha}{G(k)}\\&\times\exp[\mathrm{i}(kx+\beta z-\omega t)]\,\mathrm{d}k\mathrm{d}\omega,\end{aligned}\tag{3}$$

where ω is the angular frequency, k is the wave number in x-direction, i is the unit imaginary number, $\alpha=(k_{\mathrm{p}}^2-k^2)^{1/2}$, $\beta=(k_{\mathrm{s}}^2-k^2)^{1/2}$, k_{p} and k_{s} are the wave numbers of the p and SV waves, μ is Lame's constant, $F(\omega)$ is the Fourier transformation of $f(t)$, and $G(k)=4k^2\alpha\beta+(k_{\mathrm{s}}^2-2k^2)^2$.

The displacement components can be easily obtained by the function of displacement potentials,

$$\begin{aligned}u_x(x,z,t)&=\frac{\partial\varphi(x,z,t)}{\partial x}-\frac{\partial\psi(x,z,t)}{\partial z},\\u_z(x,z,t)&=\frac{\partial\varphi(x,z,t)}{\partial z}+\frac{\partial\psi(x,z,t)}{\partial x},\end{aligned}\tag{4}$$

where $u_x(x,y,t)$ and $u_z(x,y,t)$ are the displacement components in x and z directions.

For the convenience of analysis, the above formula of displacement components can be rewritten in polar coordinates as

$$\begin{aligned}u_x(r,\theta,t)&=u_x(x,z,t)=u_x(r\sin\theta,r\cos\theta,t),\\u_z(r,\theta,t)&=u_z(x,z,t)=u_z(r\sin\theta,r\cos\theta,t).\end{aligned}\tag{5}$$

2.2. Beam focusing field of SV waves

As shown in Fig. 4, the linear phased array consisting of N elements is placed on the free surface (N is an even number), where the origin of the coordinate system is located at the center of the whole array and the elements are numbered sequentially. Assume that the inter-element spacing is d, and the element width is $2a$. Any arbitrary observation point inside the medium is denoted as (x, z) or (r, θ). In addition, the focal point is located at (x_{f}, z_{f}) or (r_{f}, θ_{f}) with the focal length r_{f} and the steering angle for beam focusing θ_{f}. Here the anticlockwise angles with respect to the z-axis are taken to be positive, which means that the azimuth angle θ and steering angle θ_{f} plotted in Fig. 4 are positive.

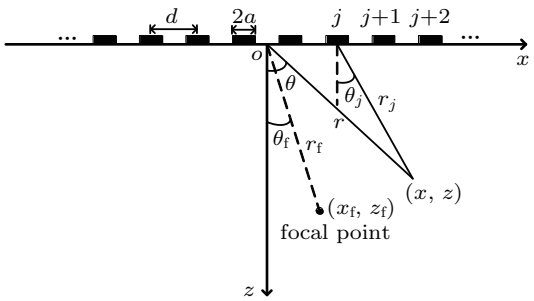


Fig. 4. Modeling of a transducer array of N elements for the beam focusing field.

The geometric relationships in Fig. 4 can be given as the following formulas:

$$\begin{aligned}r_j&=\sqrt{r^2-2r\left(j-\frac{N+1}{2}\right)d\sin\theta+\left(j-\frac{N+1}{2}\right)^2d^2},\\\theta_j&=\arctan\frac{r\sin\theta-\left(j-\frac{N+1}{2}\right)d}{z}.\end{aligned}\tag{6}$$

As observed in Fig. 4, the SV waves for focusing can be regarded to travel in straight lines without refraction or wave

mode conversion, which makes it easier to determine the time delays on the j-th element required for beam focusing of SV waves,

$$\tau_j = \frac{1}{c_s}\left\{\left(r_f \sin\theta_f + \frac{N-1}{2}d\right)^2 + (r_f\cos\theta_f)^2\right\}^{1/2} - \frac{1}{c_s}\left\{\left(r_f\sin\theta_f + \frac{N+1-2j}{2}d\right)^2 + (r_f\cos\theta_f)^2\right\}^{1/2}. \quad (7)$$

Then, the focusing field of SV waves for the linear phased array can be considered as the superposition with the contribution of all elements,

$$u_x^s(r,\theta,t) = \sum_{j=1}^{N} u_x(r_j,\theta_j,t-\tau_j),$$
$$u_z^s(r,\theta,t) = \sum_{j=1}^{N} u_z(r_j,\theta_j,t-\tau_j). \quad (8)$$

Note that for the case of $t-\tau_j < 0$, the above displacement components are equal to zero.

2.3. Radiation directivity

With the formulas of displacement components (8), the total displacement can be written as

$$U(r,\theta,t) = \sqrt{[u_x^s(r,\theta,t)]^2 + [u_z^s(r,\theta,t)]^2}. \quad (9)$$

In practical employment of phased array, the elements are excited by the short-time pulse to generate transient waves. In this paper, the cosine envelope function with finite duration is selected as the excitation source in an attempt to make the field more realistic, which is introduced in detail later. Therefore, in order to analyze the transient beam focusing characteristics, the radiation directivity function is defined as

$$H(\theta) = \frac{\max[U(r_f,\theta,t)]}{\max[U(r_f,\theta_f,t)]}, \quad (10)$$

where $U(r_f,\ \theta,\ t)$ is the total displacement at a given focal length r_f and any arbitrary angle θ, $U(r_f,\ \theta_f,\ t)$ is the total displacement at the same focal length r_f and the steering angle θ_f, and max[ ] is an operator that takes the peak amplitude of total displacement within all calculation time t. This definition of directivity function ensures that the influence of other waves propagating in the medium on the focusing performance of SV waves can be taken into account.

3. Beam focusing performance of SV waves

In this section, the variation of the beam focusing performance of SV waves for parameters is analyzed in detail through numerical simulation, including the element width ($2a$), inter-element spacing (d) and steering angle (θ_f). The numerical results show the critical conditions for achieving good focusing performance of SV waves for contact-type linear array. This paper only focuses on the bulk waves radiating inside the medium, which makes the Rayleigh waves neglected in the calculation hereafter.

As mentioned above, a cosine envelope function is chosen as the excitation source in an attempt to simulate the realistic focusing field, which can be written as

$$f(t) = \frac{1}{2}\left\{1+\cos\left[\frac{2\pi}{t_c}\left(t-\frac{t_c}{2}\right)\right]\right\} \times \cos\left[2\pi f_0\left(t-\frac{t_c}{2}\right)\right], \quad 0 \leqslant t \leqslant t_c,$$
$$f(t) = 0, \quad t<0,\ t>t_c, \quad (11)$$

where f_0 is the central frequency, and t_c is the pulse duration. In the simulation, the parameters are selected as $f_0 = 1.5$ MHz and $t_c = 2/f_0$, and the transient waveform of cosine envelope is plotted in Fig. 5. The inspection medium is chosen to be steel, where the velocities of p and SV waves are 5778 m/s and 3194 m/s, respectively. The wavelengths of p and SV waves corresponding to the central frequency are $\lambda_p = 3.8$ mm and $\lambda_s = 2.1$ mm.

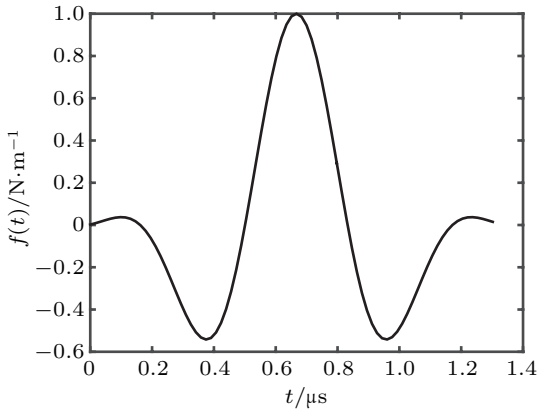


Fig. 5. The waveform of the cosine envelope function with $f_0 = 1.5$ MHz and $t_c = 2/f_0$.

3.1. Excitation and propagation mechanism of SV waves

As analyzed in previous works,[10,11] the basic radiation directivity of a single element plays an important role in the focusing field. This illustrates that the beam focusing performance of SV waves is significantly dependent on the radiation directivity of the single element. Thus, it is critical to study the excitation characteristics of SV waves radiated by a single element. As shown in Fig. 6, the transient directivity patterns of the field excited by a single element with different widths are given. This demonstrates an important property of the SV wave that its transient radiation directivity is determined by the element size. One can be observed that the SV waves generated by the element mostly radiate along higher azimuth angles but barely propagate forward. This unique excitation and propagation mechanism of SV waves enables the linear phased array to achieve good beam focusing performance of SV waves at higher steering angles instead of lower steering angles. However, as the element size enhances, the azimuth angle with peak amplitude of SV waves gradually decreases.

Worse still, there exists the erratic fluctuation in the basic directivity pattern of SV waves for a larger element size, which may make a deleterious effect on the focusing performance. Furthermore, it is also shown that the narrower element can generate the SV waves with amplitude higher than p-waves. Thus, it is recommended to employ the element with smaller size in terms of beam focusing performance of SV waves.

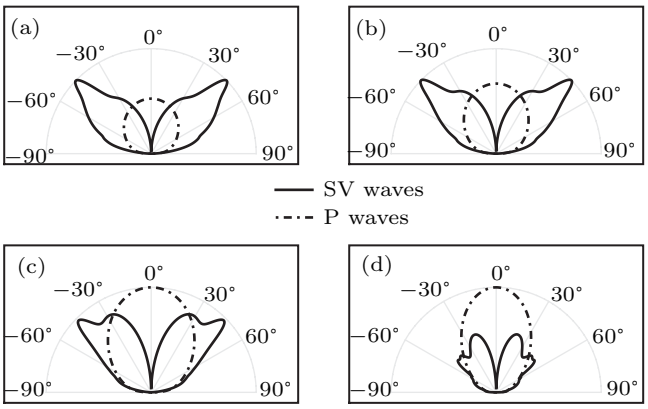


Fig. 6. The transient directivity patterns of SV waves and p-waves excited by a single element with various widths: (a) $2a/\lambda_s = 0$ (point like source), (b) $2a/\lambda_s = 0.5$, (c) $2a/\lambda_s = 1.0$, (d) $2a/\lambda_s = 1.5$.

It should be noted that since the element in this paper is excited to generate transient waves, the basic directivity patterns given above differ from that in previous studies, where the element was assumed to emit continuous waves.[15,20,27] This also indicates the differences between the acoustic fields radiated by transient waves and by continuous waves.

3.2. Element width ($2a$)

As analyzed above, the element width has a decisive influence on the beam focusing performance of SV waves. Thus, figure 7 shows the beam focusing performance of SV waves for linear phased array with different element sizes at three steering angles. In the figure, the main lobe is defined as the lobe appearing at the steering angle, which is surrounded by lobes with lower amplitudes called the side lobes. In general, the narrower main lobe provides the higher imaging resolution and more concentrated focusing energy, which implies the better beam focusing performance. It is desirable to suppress the side lobe amplitude, which implies the reduction of focusing energy leakage.

It can be observed that the main lobe quality degrades and the side lobe amplitude increases with the growth of element size. There even exists the erratic fluctuation in the main lobe for the case of $2a = 1.5\lambda_s$, which may result in the confusing signal. This phenomenon can be explained by the basic radiation directivity of SV waves shown in Fig. 6.

In addition, it is desirable to acquire the highest energy of acoustic waves at the predetermined focal point, which is helpful to accurately employ the focal spot with highest energy to perform inspection. However, it was found that the peak amplitude of displacement in field may not occur at the predetermined focal point due to the diffraction effects.[13] Thus, the distribution of acoustic field along steering direction is also an important criterion for evaluating the beam focusing performance. As shown in Fig. 8, the enlargement of element width can result in the deviation of highest energy from the predetermined focal point, as well as the erratic fluctuation of focusing energy around focal point. Thus, it can be argued that the narrower element is able to provide the better beam focusing performance of SV waves.

However, it should be noted that the element with smaller size makes a strict requirement for the manufacturing technology of arrays and suffers from a penalty of lower focusing energy. Fortunately, it can be observed that the influences of element size on the profile of the radiation directivity of SV waves for a relatively smaller element width is marginal, which can be proved by Figs. 6(a) and 6(b). In other words, the reasonable enlargement of element width can achieve good beam focusing performance without sacrificing the focusing energy. Therefore, it is recommended to employ an element width larger than $0.4\lambda_s$ but smaller than λ_s for the particular case in this paper.

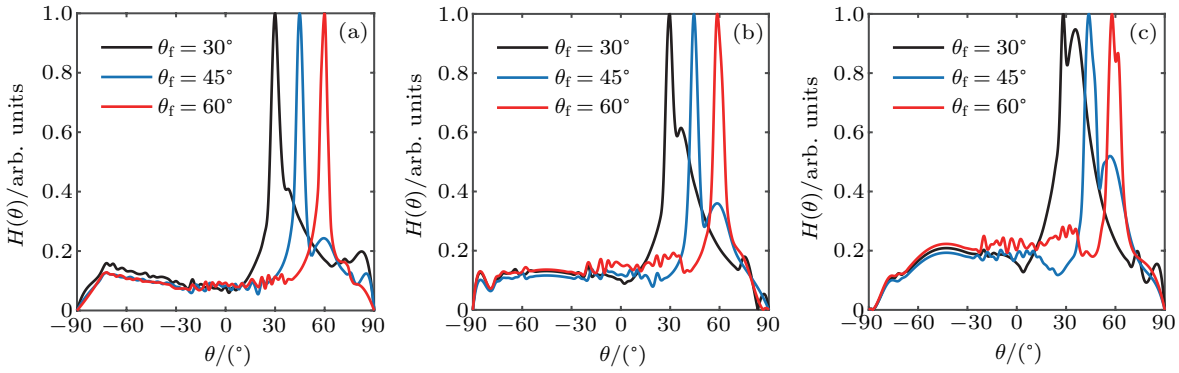


Fig. 7. The directivity patterns of beam focusing field of SV waves excited by contact-type linear phased array for various element widths: (a) $2a/\lambda_s = 0.5$, (b) $2a/\lambda_s = 1.0$, (c) $2a/\lambda_s = 1.5$ ($N = 32$, $d = 1.5\lambda_s$, $r_f = 40$ mm).

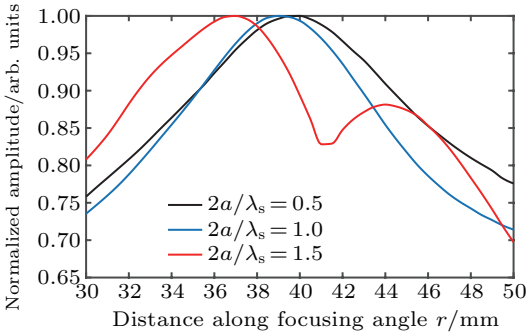


Fig. 8. The distribution of displacement amplitude along steering direction for various element widths ($N = 32$, $d = 1.5\lambda_s$, $r_f = 40$ mm).

3.3. Inter-element spacing (d)

The inter-element spacing is another important design parameter of the transducer array that has an important effect on the focusing performance. As shown in Fig. 9, the variations of beam focusing performance for various inter-element spacing are given, where the element width is selected to be $0.5\lambda_s$.

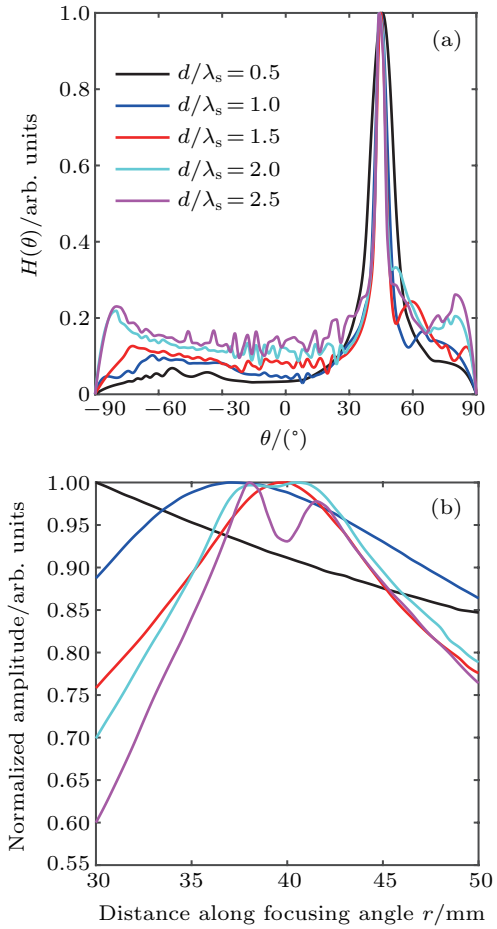


Fig. 9. The beam focusing performance of SV waves for various inter-element spacings: (a) directivity patterns of focusing field, (b) the distribution of displacement amplitude along steering direction ($N = 32$, $2a = 0.5\lambda_s$, $r_f = 40$ mm, $\theta_f = 45°$).

In general, the beam focusing or steering performance of linear phased array can profit from the reasonable enlargement of inter-element spacing.[10–12] This effect is similar to the benefit from the enlargement of the overall dimension of the monolithic transducer. Therefore, one can observe from Fig. 9(a) that as the inter-element spacing increases, the main lobe quality improves slightly. It is shown in Fig. 9(b) that for the smaller value of inter-element spacing ($d/\lambda_s < 1.5$), the location of peak amplitude approaches asymptotically to the focal point with the growth of inter-element spacing. Subsequently, the continuous enlargement of inter-element spacing may lead to the excessively large distance between the elements and the focal point, so that the elements away from the focal point cannot make the effective contributions. As a consequence, this results in the erratic fluctuation of focusing energy, such as the case of $d/\lambda_s = 2.5$ in Fig. 9(b). In conclusion, it is recommended to employ the inter-element in the range of λ_s and $2\lambda_s$ for the good beam focusing performance in such a particular case.

3.4. Steering angle (θ_f)

As mentioned above, it is critical to achieve good beam focusing performance of SV waves at higher steering angles. Thus, the variations of directivity patterns of focusing field for various steering angles are plotted in Fig. 10(a).

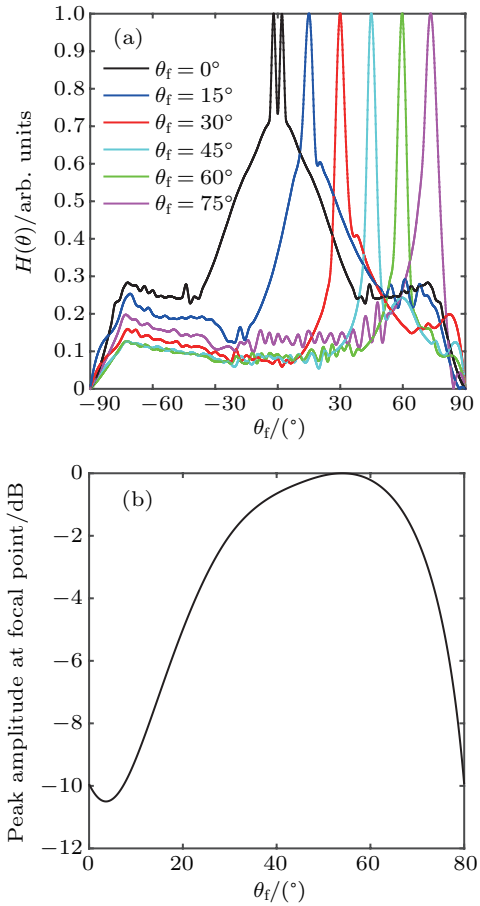


Fig. 10. The beam focusing performance of SV waves for various steering angles: (a) directivity patterns of focusing field, (b) beam focusing energy distribution ($N = 32$, $2a = 0.5\lambda_s$, $d = 1.5\lambda_s$, $r_f = 40$ mm).

One can be observed that for lower steering angles, the main lobe quality is significantly improved with increasing steering angles. The main lobe quality converges to optimum when the beam is steered in the range from 30° to 60°. After

that, the main lobe quality has a tendency to degrade. This phenomenon is exactly consistent with the radiation directivity pattern shown in Fig. 6(b), where the SV waves primarily radiate along $|\theta| = 45°$.

In order to deeply analyze the beam focusing performance at various steering angles, figure 10(b) gives the distribution of focusing energy at the focal point for various steering angles. It is shown that the beam focusing of SV waves can generate higher focusing energy at the focal point with steering angle in the range of 30° to 70°, which can provide high signal-to-noise ratio for inspection. This illustrates that the available inspection area for the beam focusing of SV waves is located in such a range.

4. Conclusion and perspectives

In this paper, the transient beam focusing behavior of SV waves for the contact-type linear phased array is studied. With the angular spectrum method, the theoretical formulas of the beam focusing field of SV waves excited by a contact-type linear phased array is derived. The numerical model is developed to analyze the beam focusing characteristics of SV waves, where the elements are excited by a cosine envelope function to generate transient waves in an attempt to make the simulated field more realistic.

The numerical results show that the SV waves excited by the element radiate into the solid primarily along high azimuth angles rather than forward. This unique excitation and propagation characteristics of SV waves enables the contact-type linear phased array to achieve good beam focusing performance of SV waves at high steering angles. The transient radiation directivity of SV waves is determined by the element width. It can be concluded that a larger element size degrades the main lobe quality and results in the erratic fluctuation of focusing energy around focal point, which makes a deleterious effect on the beam focusing performance. Instead, the narrower element can provide better beam focusing performance of SV waves. However, it should be noted that the element with smaller size suffers from a penalty of lower focusing energy.

The investigation is also extended to study the influence of inter-element spacing on the beam focusing performance. In conclusion, the reasonable enlargement of inter-element spacing can significantly improve the focusing performance of transducer array, while the excessively large inter-element spacing ($d/\lambda_s > 2.0$) may also result in the erratic fluctuation of focusing energy around focal point. As a result, the element width in the range of $0.4\lambda_s$ and λ_s and the inter-element in the range of λ_s and $2\lambda_s$ are recommended to be employed for optimum beam focusing performance in this paper. Furthermore, the contact-type linear phased array can provide higher focusing energy of SV waves for the available inspection area with a steering angle in the range from 30° to 70°.

In summary, the beam focusing technology of SV waves for the contact-type linear phased array can meet the requirements of inspections for various components with complicated structures, and overcome the disadvantages of conventional wedge transducer array.

References

[1] Tan J S, Frizzell L A, Sanghvi N, Wu S, Seip R and Kouzmanoff J T 2001 *J. Acoust. Soc. Am.* **109** 3055
[2] Karaman M, Wygant I O, Oralkan O and Khuri-Yakub B T 2009 *IEEE Trans. Med. Imag.* **28** 1051
[3] Matte G M, Van Neer P L M J, Danilouchkine M G, Huijssen J, Verweij M D and de N 2011 *IEEE Trans. Ultrason. Ferroelectr. Freq. Contr.* **58** 533
[4] Bucci O M, Crocco L, Scapaticci R and Bellizzi G 2016 *Proc. IEEE.* **104** 633
[5] Chatillon S, de Roumilly L, Porre J, Poidevin C and Calmon P 2006 *Ultrasonics* **44** e951
[6] Dupont-Marillia F, Jahazi M, Lafreniere S and Belanger P 2019 *NDT&E Int.* **103** 119
[7] Choi Y, Lee H, Hong H and Ohma W S 2011 *J. Acoust. Soc. Am.* **130** 2720
[8] Zhang J, Yu P and Gang T 2016 *Nondestr. Test. Eval.* **31** 303
[9] Lerch T P, Schmerr L W and Sedov A 1997 *Review of progress in quantitative nondestructive evaluation* vol 16 p 885
[10] Wooh S C and Shi Y J 1999 *Wave Motion* **29** 245
[11] Wooh S C and Shi Y J 1998 *Ultrasonics* **36** 737
[12] Wooh S C and Shi Y J 1999 *J. Nondestruct. Eval.* **18** 39
[13] Azar L, Shi Y J and Wooh S C 2000 *NDT&E Int.* **33** 189
[14] Huang R and Schmerr L W 2009 *Ultrasonics* **49** 219
[15] Lee J H and Choi S W 2000 *IEEE Trans. Ultrason. Ferroelect. Freq. Contr.* **47** 644
[16] Crowther P 2004 *Insight-Non-Destruct. Test. Cond. Monit.* **46** 525
[17] Yang S, Yoon B and Kim Y 2009 *NDT&E Int.* **42** 128
[18] Ye J, Kim H, Song S, Kang S, Kim K and Song M 2011 *NDT&E Int.* **44** 290
[19] Lhémery A, Calmon P, Lecœur-Taïbi I, Raillon R and Paradis L 2000 *NDT&E Int.* **33** 499
[20] Drinkwater B W and Wilcox P D 2006 *NDT&E Int.* **39** 525
[21] Kim H J, Park J S, Song S J and Schmerr Jr L W 2004 *J. Nondestr. Eval.* **23** 81
[22] Song S J and Kim C H 2002 *Ultrasonics* **40** 519
[23] Dai Y X, Yan S G and Zhang B X 2019 *Acoust. Phys.* **65** 235
[24] Noroy M, Royer D and Fink M A 1995 *IEEE Trans. Ultrason. Ferroelect. Freq. Contr.* **42** 981
[25] Zhang B X, Liu D D, Shi F F and Dong H 2013 *Chin. Phys. B.* **22** 014302
[26] Schafer M E and Lewin P A 1989 *J. Acoust. Soc. Am.* **85** 2202
[27] Wooh S C, Zhou Q and Wang J 2003 *Exp. Mech.* **43** 450